COBEM 2023 27TH INTERNATIONAL CONGRESS OF MECHANICAL ENGENEERING

ABCM Brazilian Society of Mechanical Sciences and Engineering
27th ABCM International Congress of Mechanical Engineering
December 04-08, 2023, Florianópolis-SC, Brazil

COBEM2023-1436
FLUID-STRUCTURAL NUMERICAL EVALUATION OF THE EFFICIENCY OF A FLOW ATENUATOR DEVICE THROUGH VARIATIONS IN THE MODULUS OF ELASTICITY

Pedro Henrique Bergamim Bis
Matheus Campos Vieira
Gustavo Cordeiro Barreiros
João Paulo Barbosa
Renato do Nascimento Siqueira
Ayrton Cavallini Zotelle
Instituto Federal do Espírito Santo – Campus São Mateus – Rodovia BR 101 Norte, km 58 – Litorâneo – CEP 29.932-540 – São Mateus – ES
pedrobbis@hotmail.com
matheuscamposvieira@hotmail.com
guicordeiro42@gmail.com
jpbarbosa@ifes.edu.br
renatons@ifes.edu.br
ayrton.zotelle@ifes.edu.br

Abstract. *In many industrial conditions, positive displacement pumps are used to move fluids with high viscosity or over long distances. In this type of pump, the liquid receives pressure energy through the action of forces directly linked to the movement of a piston or diaphragm, resulting in discharge flows that have a pulsating characteristic, which generates vibration and wear problems in the piping system. Flow atenuators are devices that operate based on an energy absorption and restitution mechanism to promote stability in pulsating flows and mitigate the effects caused by positive displacement pumps. Among the attenuators available on the market, the models that use inflatable gaseous fluid are the most used, however, they are dependent on thermodynamic parameters that make their use unfeasible in certain industrial activities. Thus, this work aims to contribute to the development of the study of attenuators that operate through an elastic structure, numerically analyzing the influence of the variation of the modulus of elasticity in 1, 2, 3, 4 and 5 MPa in the efficiency of mitigation. For this, the three-dimensional model of fluid-structure interaction implemented in the commercial software Ansys® Workbench 2020 R1 was used. The iterations of the simulations were scaled between two solvers: one for the structural analysis, based on the finite element method (FEM), and another for the calculation of computational fluid dynamics (CFD), which together modeled the turbulent flow of water at a Reynold's 3820 under a cylindrical deformable frame 400 mm long, 1 3/8" in diameter and 1 mm thick. The results demonstrate that the reduction of the modulus of elasticity of the material used as a continuous deformable medium of the attenuator causes an increase in the absorption capacity and energy restitution and consequently a higher level of attenuation. The best values are found for the 1 MPa case, which presents an attenuation level close to 77% of the inlet flow, a value that corresponds to a 37% increase in attenuation in relation to the 5 MPa case.*

Keywords: *Simulation. Flow attenuators. Elastic modulus. Fluid-structural.*

1. INTRODUCTION

In many industrial pumping systems, the need arises to move fluids over long distances or with high viscosity. In these occasions, conventional pumps, also known as turbopumps, are not able to overcome the head losses caused by these flows. To deal with this challenge, the use of positive displacement pumps is recommended (Macintyre, 1997).

Positive displacement pumps, also called volumetric pumps, can be classified into two main types: rotary and reciprocating. Specifically in reciprocating pumps, the movement of the propeller generates a flow with intermittent characteristics, resulting in pulsations that cause vibration and noise. These effects can compromise the useful life of the installation due to wear and fatigue (Beynart, 1999; Shaaban and Mohany, 2015). Therefore, there is a need for equipment capable of attenuating pulsations and mitigating the aforementioned problems.

Pulsation dampers, also known as attenuators or accumulators, are used to reduce pressure and flow pulses (Koegler et al., 2016; Deng et al., 2012). There are several models of these devices described in the literature, which can be classified according to their operating principle, as resistive, reactive or composite attenuators (Wang et al., 2021).

Resistive dampers dissipate the energy of fluid pulsations through friction, similarly to resistive sound dampers, which use highly permeable absorbent materials to reduce noise (Wang et al., 2021). Although they are effective in suppressing pressure spikes, resistive attenuators cause considerable energy loss due to their operating principle.

On the other hand, reactive attenuators operate through the implementation of a chamber or branch connected to the discharge line. The characteristics of this chamber define its subtype, which can be interference, resonance or expansion. Interference-type reactive attenuators take advantage of the principle of superposition and interference between harmonics to achieve the objective of mitigating pulsations. However, the large space occupied by these devices and the narrow working frequency range reduce their use. Expansion chamber type attenuators are easier to install and have reduced geometry. However, the release of energy from the pulsations of the liquid through the sudden expansion and compression of the fluid restricts its application to high frequencies. Attenuators that work by absorbing and returning energy through compression of a continuous medium (fluid or solid) are called reactive pulsation attenuators that operate by resonance (Koegler et al., 2016; Wang et al., 2021).

Among the types and subtypes of accumulators mentioned, the most widespread on the market are those that operate reactively by resonance and use an inflatable gaseous fluid as a deformable medium. However, these devices have their performance affected by thermodynamic characteristics inherent to the volume of gas contained in their interior (Wachel and Price, 1988). Therefore, the use of attenuators that absorb and restore energy through their solid structure becomes more interesting, since they dispense with the constant gas charge, are easy to install and require less maintenance.

In general, elastomeric materials are used as a means of storing and restoring energy in accumulators. Its viscoelastic properties, combined with the low Young modulus (Shahzad et al., 2015), ensure efficiency in the attenuation process.

There are two types of elastomers: synthetic and natural. Synthetic elastomers, derived from petroleum, are highly resistant to degradation. Natural elastomers, more commonly used in attenuators (Flexodamp; Flowrox, 2015), are produced through latex coagulation and need to be chemically improved to achieve the desired mechanical characteristics. Among the methods used to improve natural elastomers, the addition of sulfur, through the vulcanization process, allows the variation of an important parameter that influences the dynamic behavior of the attenuator: the Young modulus (Callister, 2007).

The Young modulus is a mechanical property of materials that measures stiffness and ability to return to original shape after deformation (Callister, 2007). The material used in the fabrication of the attenuator needs to have an adequate Young modulus to withstand flow fluctuations without suffering structural failure and efficiently dissipate the energy of flow pulses. A very low Young modulus can result in an overly springy response, leading to insufficient damping. On the other hand, high a Young modulus can make the attenuator stiff, making it difficult to properly absorb energy.

Thus, the choice of modulus of elasticity of the material used in manufacturing the attenuator plays a crucial role in determining the level of attenuation. Therefore, the present study aims to analyze, using numerical tools, how the variation in the modulus of elasticity affects the attenuation of flow peaks caused by positive displacement pumps. In addition, we seek to determine the relationship between the volumetric variation and the level of attenuation achieved, as well as to evaluate the impact of this variation in the modulus of elasticity on possible structural failures.

2. METHODOLOGY

A three-dimensional fluid-structure interaction model was implemented using the commercial software Ansys® Workbench 2022 R2. Two different solvers were used: one dedicated to the calculation of computational fluid dynamics (CFD) and another for structural analysis based on the finite element method (FEM). Fluid pressure excitation was incorporated into the Ansys® Fluent software, which employs the finite volume method for domain discretization. The structure's responses were obtained through Ansys® Mechanical, which uses a finite element approach to solve dynamic equations. The simulations were conducted with the aid of the Ansys® System Coupling bidirectional coupling solver, which handles fluid pressure and structure deformation. To integrate the fluid and solid domains over time in a fluid-structure interaction (FSI) simulation, a partitioned coupling approach was employed (Figure 1). This method involves the independent resolution of the fluid and solid equations, followed by the exchange of information between these two parts at each time step, thus ensuring the coherence and convergence of the global solution.

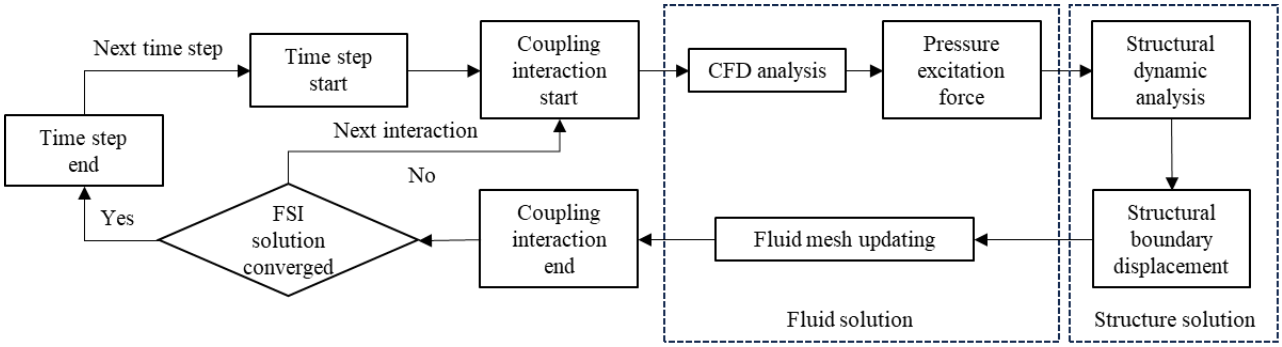

Figure 1. Flowchart of the fluid-structure iteration simulation process.

2.1 Geometry, initial conditions and boundary conditions

The geometry adopted in the simulations was based on reactive flow attenuators marketed by Flexodamp and Flowrox (2015). The model was created with a geometry of 400 mm in length and 34.92 mm in diameter, representing the volume traveled by the fluid inside the attenuator. From the outer surface of the main cylinder wall, a new elastic surface has been added that represents the attenuator's deformable zone. This surface is 1 mm thick and was modeled as a shell element, following the theory of thin-walled pressure vessels, $^{E}/_{R} > 10$ (Hibbeler, 2000).

In addition to the main cylinder and the deformable surface, a tube with a diameter of 25.4 mm and a length of 50 mm was added upstream of the attenuator. This tube represents the hydraulic system before the attenuator and was used to apply the fluid ingress condition. In the same way, downstream of the attenuator, another tube with a diameter of 25.4 mm and a length of 50 mm was modeled. In the center of this tube, a plane was defined that was later used to apply the equivalent pressure drop condition to the hydraulic system after the attenuator. In order to reduce the computational cost of the simulations, it was decided to use the condition of symmetry in the XZ and YZ planes (Figure 2).

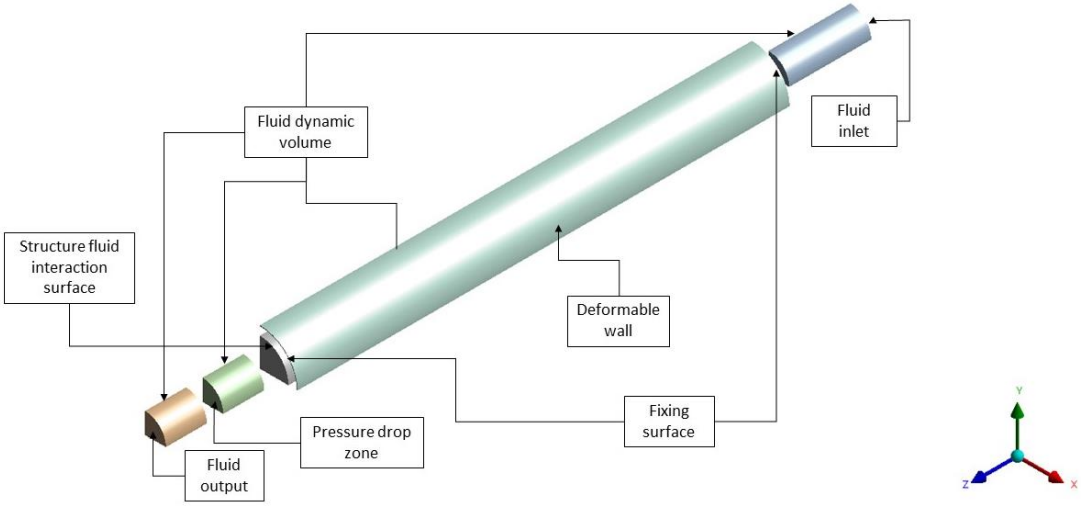

Figure 2. Exploded view of the geometric structure used in the flux attenuator simulations, showing the different areas of the domain.

After determining the geometry to be studied, the relevant initial conditions for the simulation were established. The flow was modeled as two-dimensional, incompressible, Newtonian and turbulent. The necessary fluid dynamic properties, together with their respective parameters, are described in Table 1.

Table 1. Initial conditions and parameters used in the implementation of the fluid dynamic model.

Turbulence model		k - ε
Pressure and velocity coupling		Coupled
Mesh spatial discretization		Gradient
Mesh spatial discretization Transient formulation	Pressure	Based on least squares cells
	Moment	Second order
	Implied first order	Second upstream order
Type of solver		Controlled by the program
Formulation for large displacements		Enabled
The working fluid		Water
Specific mass (ρ)		998 Kg/m³
Dynamic viscosity (μ)		1,003E10-3
Average Reynolds		3820

To simulate the flow generated by positive displacement pumps, a velocity function (Equation 1) defined by parts in the inlet region was implemented.

$$u(t) = \begin{cases} 0{,}112, & se\ t < 2 \\ 0{,}112 + 0{,}056\ sen(7{,}086t - 14{,}172), & se\ t \geq 2 \end{cases} \quad (1)$$

In the wall region, the fluid is subject to the no-slip condition, which means that the velocity is zero. In the area where the pressure drop occurs, a permeable "thin membrane" with high head loss was inserted inside the fluid domain. This membrane is modeled using a porous jump condition, which imposes a head loss equivalent to that of the components of the hydraulic system downstream of the attenuator.

The porous medium has a finite thickness over which the pressure change (Δp) is defined by means of the Darcy-Forchheimer Law:

$$\Delta p = -\left(\frac{\mu}{\alpha}u + C_2 \frac{1}{2}\rho\, u^2\right)\Delta m \quad (2)$$

Where, α is the facial permeability of the medium, u the average velocity of the fluid, Δm thickness of the porous medium, C_2 the pressure jump coefficient, Δp is the pressure difference, ρ is the specific mass and μ is the dynamic viscosity.

A value of 2100 Pa was established for the pressure difference downstream of the attenuator's hydraulic system, resulting in a specific permeability of the medium of 1.57 x 10-6 m².

In the solid domain, the ends of the deformable wall were fixed and subjected to a zero displacement condition. The intersection between the deformable wall and the fluid dynamic volume forms the fluid-structure interaction surface. In structural terms, the attenuator thickness was modeled as a thin-walled cylindrical pressure vessel with a 1 mm thick shell. In the deformable zone of the solid domain, an elastic material with a linear stress-strain curve was assigned. The Young modulus was varied between 1 and 5 MPa, while the Poisson coefficient was defined as 0.45. To ensure the convergence of the simulations without pressure and displacement problems, a time interval of 0.1 s was established, with a minimum of 5 iterations and a maximum of 20 iterations per time interval.

2.2 Attenuation efficiency

Given that the performance of the attenuator leads to a decrease in the amplitude of the output velocities in relation to the input, the effectiveness of the device is evaluated by means of an attenuation factor (Fa), which can be calculated using the following equation:

$$Fa = \left(1 - \sqrt{\frac{\int_0^t (v_{out}(t) - v_{ave})^2 dt}{\int_0^t (v_{inl}(t) - v_{ave})^2 dt}}\right) 100 \quad (3)$$

The v_{inl} parameter represents the input speed, v_{ave} refers to the average speed and v_{out} represents the system output speed. When dealing with a pulsating flow, the attenuation factor (Fa) is used to evaluate the performance of the device. In this context, a value of Fa equal to 100% indicates a completely stable flow rate at the outlet, which means that the variation in velocity is minimal. On the other hand, a value of Fa equal to 0% indicates that there are no stabilization effects, that is, the inflow profile remains unchanged, with no reduction in the amplitude of the outflow velocities.

2.3 Computational mesh

To establish a link between structural and fluid meshes in a fluid-structure interaction (FSI) simulation, the coupling method known as Arbitrary Lagrangian-Eulerian - ALE was adopted. In this method, the structural mesh is shifted to align with the fluid mesh at each time interval, allowing the transfer of physical field values, such as velocity and pressure, between the meshes through interpolation.

To ensure results independent of domain discretization, tests were conducted with computational meshes in both fluid dynamics and structural analyses. In the structural model, five distinct meshes were tested, varying the relationship between the length and width of the elements. The average of the displacements obtained over time at a specific point on the attenuator wall was compared. All mesh arrangements showed variation in the results of less than 1%. However, based on the trend of the curve that relates the number of elements to deformation, the mesh composed of 52,057 nodes and 51,084 elements was chosen (Figure 3).

In the fluid domain, the influence of four mesh models on the percentage of attenuation (Equation 3) was analyzed, varying the longitudinal length by 1, 2, 3 and 4 mm. The selection of the 3 mm long mesh, composed of 92,475 nodes

and 120,540 elements (Figure 4), was based on the stability of the curve that relates the number of elements to the percentage of attenuation.

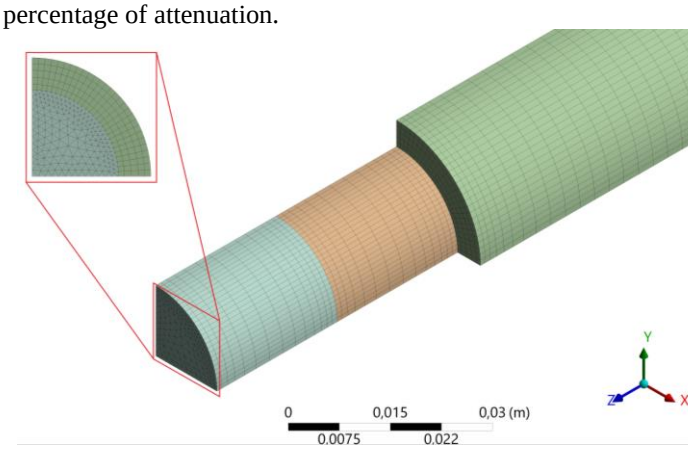

Figure 3. Fluid dynamic mesh used in the simulations.

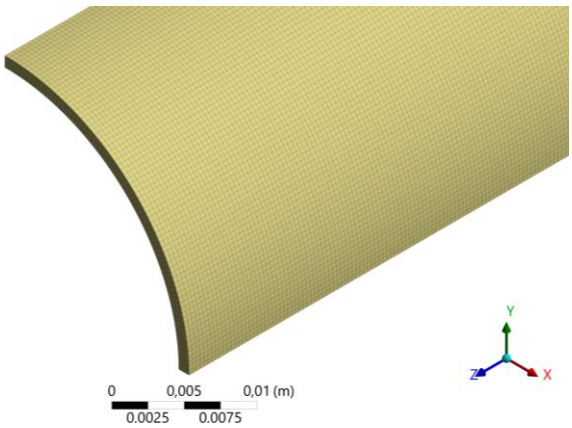

Figure 4. Structural mesh used in the simulations

2.4 Mathematical model

To address the transient flow of an incompressible fluid in a flexible tube, an arbitrary Eulerian-Lagrangian formulation was adopted. Eulerian approach is used to represent the behavior of the fluid, considering its properties over time. For an incompressible, Newtonian fluid with constant viscosity, the fundamental equations that describe its behavior in the domain are the mass conservation equation (Equation 4) and the momentum conservation equation (Equation 5) (OLIVEIRA et al., 2016):

$$\frac{\partial \rho_f}{\partial t} + \nabla\left(\rho_f \vec{U}\right) + \frac{1}{V_m}\left[\frac{\partial}{\partial t}\int_{V_c} \rho_f \, dV(t) + \int_{S_c} \rho_f \vec{U} \cdot \vec{n} \, dA(t)\right] = 0 \tag{4}$$

$$\rho_f \frac{\partial(\vec{U})}{\partial t} + \rho_f \vec{U} \cdot \left(\nabla \vec{U}\right) = -\nabla p + \mu\left(\nabla^2 \vec{U}\right) + \vec{f_f} \tag{5}$$

Where ρ_f is the fluid density, t is time, $\vec{U}$ is the velocity vector, V_m is the average volume of fluid, $\vec{n}$ is the normal vector to the surface, p is the pressure, μ is the dynamic viscosity and $\vec{f_f}$ body forces per unit volume.

On the other hand, the Lagrangian approach was used to represent the movement of the flexible tube surface, taking into account its deformation and displacement. The equations that govern the solid domain, in the case of linear structures, are based on Hooke's law (OLIVEIRA et al., 2016):

$$\rho_s \frac{\partial^2 \overrightarrow{d_s}}{\partial t^2} = \nabla \cdot \sigma_s + \overrightarrow{f_s} \tag{6}$$

$$\sigma_s = c : \varepsilon \tag{7}$$

$$\varepsilon = \frac{1}{2}\left[\left(\nabla \overrightarrow{d_s}\right) + \left(\nabla \overrightarrow{d_s}\right)^T\right] \tag{8}$$

Where ρ_s is the material density, σ_s is the second-order stress tensor, $\overrightarrow{f_s}$ is the external forces applied, c is the fourth-order stiffness tensor, $\overrightarrow{d_s}$ is the displacement vector and ε is the strain tensor.

To solve the FSI problem, which involves the Lagrangian formulation for the solid domain and the Eulerian formulation for the fluid domain, a coupling method was adopted that transfers information between the two formulations at each time step, ensuring consistency and the convergence of the global solution through two conditions.

$$\vec{d}_f = \vec{d}_s \tag{9}$$

$$\sigma_f \vec{n} = \sigma_s \vec{n} \tag{10}$$

Where $\vec{d}_f$ is the displacements of the fluid, $\vec{d}_s$ is the displacements of the solid, σ_f is the stresses of the fluid, $\vec{n}$ n is the unit normal vector to the fluid-structure interface and σ_s is the stresses of the fluid.

2.5 Validation of the model used in the flow simulations inside the attenuator

Validation of the FSI model was performed by comparing the results with a case studied by Klas et al. (2019). In this study, the authors modeled blood flow in the aorta using simulations of pulsating fluid flow in an elastic material. Several tube modeling approaches were evaluated by the authors, including constitutive relationships of linear and nonlinear mechanics, such as the Neo-Hookean and Mooney-Rivlin models of hyperelastic materials, for example.

2.5.1 Geometry, initial conditions and boundary conditions

To validate the model, a geometry similar to that used by Klas et al. (2019). The fluid dynamic domain was generated from a cylinder with a length of 500 mm and a diameter of 12.7 mm. The solid domain, in turn, was obtained by extruding 1.6 mm from the surface of the fluid-dynamic cylinder (Figure 5).

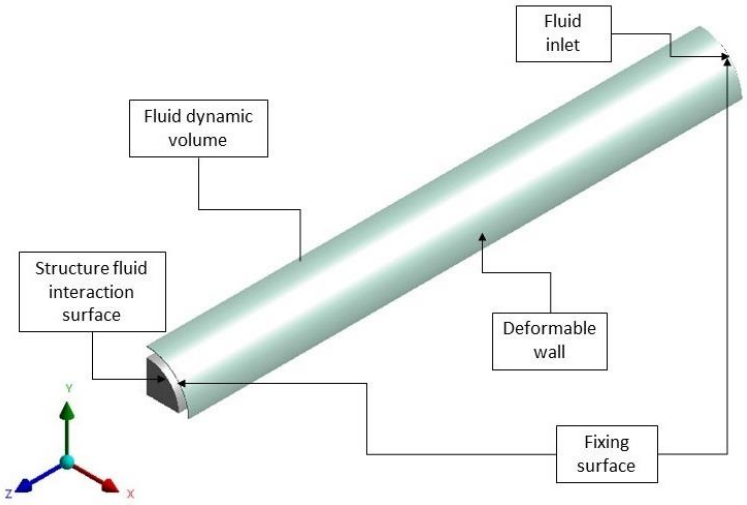

Figure 5. Exploded view of the geometry used to validate the flux attenuator.

The case studied by Klas et al. (2019) addressed the modeling of human arteries considering blood flow. For this, the authors adopted water as the working fluid, which is considered Newtonian, incompressible and turbulent (with Reynolds numbers ranging from 2000 to 30000). The physical properties of the water used were a specific mass of 998.2 kg/m³ and a dynamic viscosity of 0.001 Pa·s. The attenuator wall was simulated as a hyperelastic material using the nonlinear Mooney-Rivlin model, with coefficients C10=650000 Pa, C01=0 Pa and D1=0 Pa⁻¹.

The initial and boundary conditions established by the authors were determined based on experimental measurements and were divided into two categories: fluid dynamics and structural. In the fluid dynamic solver, pressure difference conditions were applied at the inlet (Equation 11) and at the outlet (Equation 12) of the tube. The turbulence model used was the realizable k-ε. In the wall region, a non-slip behavior was imposed between the fluid and the wall surface.

$$p_{ent}(t) = \begin{cases} 100000t, & se\ t < 0{,}5 \\ 56651{,}15 + 32296{,}73\ sen(7{,}89t - 3{,}94), & se\ t \geq 0{,}5 \end{cases} \quad (11)$$

$$p_{sai}(t) = \begin{cases} 100000t, & se\ t < 0{,}5 \\ 51015{,}15 + 32010{,}48\ sen(7{,}90t - 3{,}95), & se\ t \geq 0{,}5 \end{cases} \quad (12)$$

In the solid domain, the ends were fixed and subjected to a zero displacement condition.

The simulations progressed with a time interval of 0.1 s, performing a minimum of 5 and a maximum of 20 iterations at each interval, totaling a total time of 3.5 seconds.

3. RESULTS

3.1 Model validation results

The validation results were confronted with the studies by Klas et al. (2019), which cover the one-dimensional FSI simulation of a flexible tube using a Mooney-Rivlin solid material, experimental tests, one-dimensional FSI simulation of a flexible tube using a Neo-Hookean solid material, and a solid material described by Hooke's law.

Figure 6 shows the comparison between the external diameter variation (Δd) at a point located on the attenuator wall (x = 250, y = 6.35 and z = 0) over time.

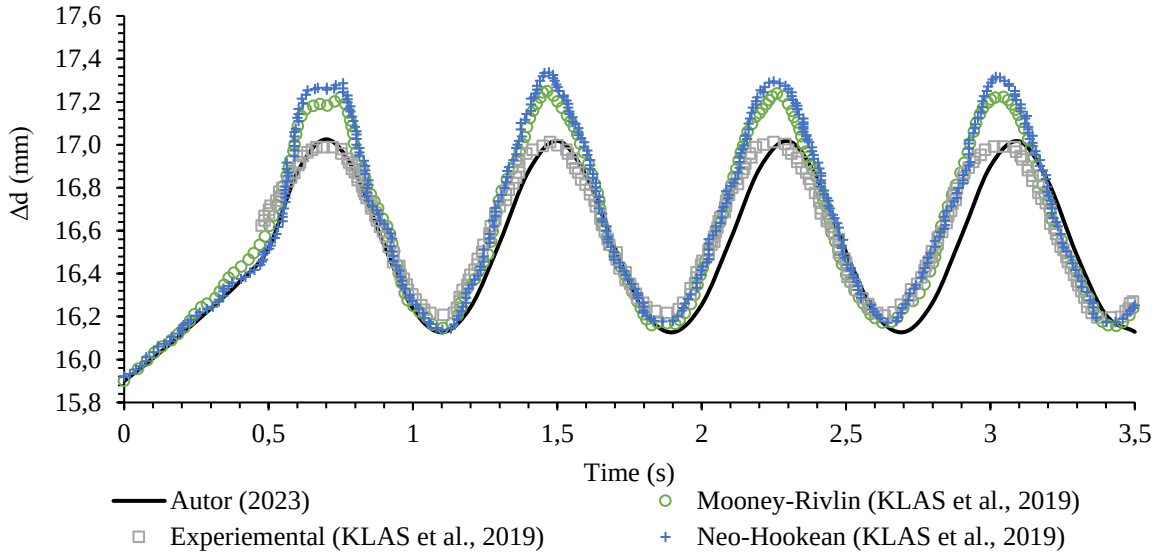

Figure 6. Comparison of the external diameter variation obtained by the author and by Klas et al. (2019).

The results demonstrate that the maximum displacement reached about 17 mm, resulting in a structural deformation of approximately 1.12 mm. The values obtained in the displacement peak region show a greater discrepancy in relation to the results of the non-linear Mooney-Rivlin model (on average 0.60%), however, when compared to the experimental tests, they present a better agreement, with an amplitude average of 0.10%.

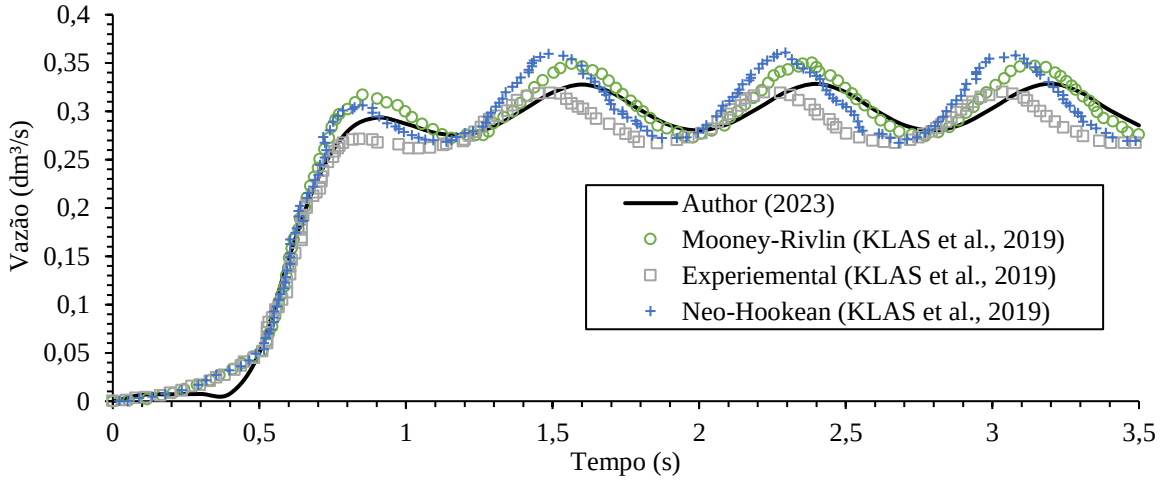

Figure 7. Comparison between flows obtained by the author and by Klas et al. (2019).

By analyzing Figure 7, we can compare the flows obtained over time. The results show that an average internal flow of about 0.35 dm³/s is reached, presenting a partial convergence with the values obtained by Klas et al. (2019). Regarding the differences between the amplitudes of the Mooney-Rivlin, Experimental and Neo-Hookean curves in comparison with the author, values of 3.72%, 3.59% and 3.18% were found, respectively. Based on the comparison of the results, it can be stated that the simulations did not present a direct agreement with the Mooney-Rivlin model. However, when compared with experimental cases or other models, such as Neo-Hookean or Hookean, they demonstrate greater consistency.

3.2 Structural stress obtained from the variation in the Young modulus

The von Mises stress distribution is presented in Figure 8 for an instant of maximum flow (t = 4.9 s) in the cases of 1 and 5 MPa. It is evident that the zone of greatest stress is located close to the model's fixation surfaces, reaching up to 96123 MPa in the case where the Young modulus is equal to 5 MPa.

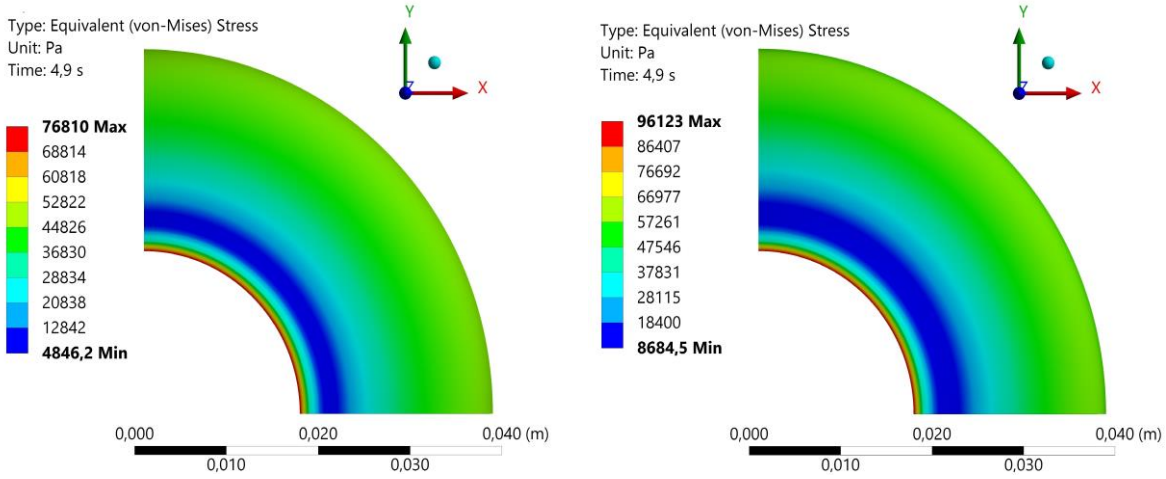

(a) E = 1 MPa (b) E = 5 MPa

Figure 8. Evaluation of the von Mises equivalent stress at peak flow, at t = 4.9 s for the 1 and 5 MPa cases.

When comparing the different simulations, it is evident that the reduction of the Young modulus from 5 MPa to 1 MPa results in a decrease in the maximum stress distribution. The maximum voltage goes from 96123 Pa to 76810 Pa, representing a reduction of approximately 20%. This decrease in voltage distribution has significant implications for resistive attenuator durability and performance. A lower voltage indicates a lower ability to withstand loads and stresses without failing, which can negatively affect attenuator life and effectiveness.

3.3 Flow pattern obtained from the variation of the Young modulus

In Figure 9, isometric views of the velocity fields inside the attenuator at different times are presented. In Figure 9 (a), which corresponds to the maximum peak flow (t = 4.9 s) with Young modulus of 1 MPa, the water enters the pipe upstream of the attenuator with a velocity of approximately 0.182 m/s. However, when passing through the attenuation duct, the velocity decreases considerably, reaching about 0.096 m/s. This reduction indicates a significant slowdown of water flow as it passes through the attenuator. In Figure 9 (b), corresponding to the flow valley (t = 5.3 s) also with Young modulus of 1 MPa, the damper is at the end of the energy restitution phase to the system. At that moment, all the fluid accumulated in the damper through the volumetric variation is expelled and added to the inlet flow. As a result, there is an increase in fluid velocity, going from 0.048 m/s (inlet) to 0.105 m/s (outlet). This velocity increase indicates that the energy stored in the damper is being released to the system, contributing to the increase in fluid velocity at the attenuator outlet.

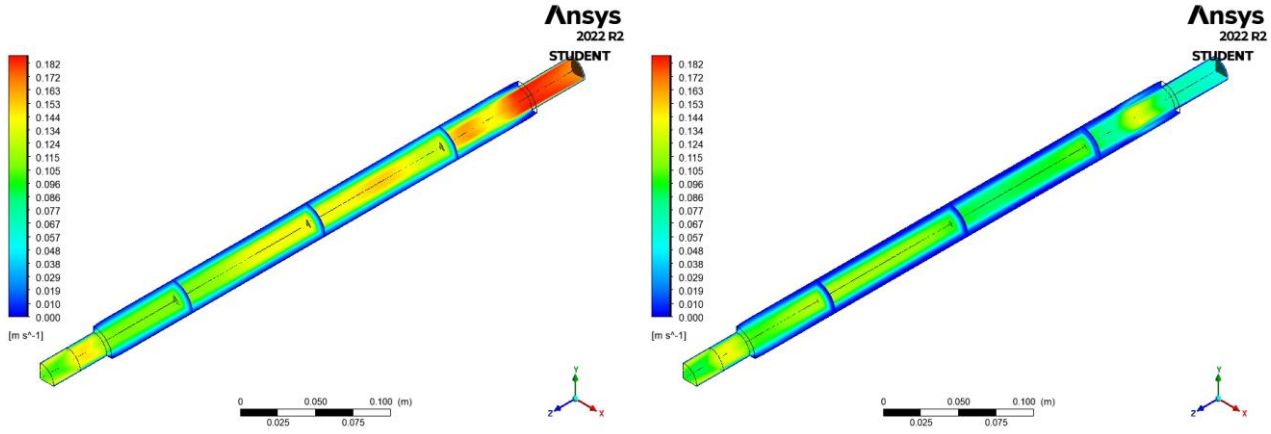

(a) t = 4.9 s (b) t = 5.3 s

Figure 9. Velocity field obtained at peak moment (t = 4.9 s) and flow valley (t = 5.3 s).

3.4 Attenuation of the flow obtained from the variation of the Young modulus

Figure 10 displays the attenuator output and input velocities, dimensionless relative to the average velocity over time. In the first two seconds of simulation, a transition period is observed, like that reported by Deng et al. (2012), in which the model progressively deforms until the fluid dynamic pressure balances with the internal tension of the material, resulting in equality between the inlet flow and the downstream flow resistance. This condition is adopted to establish a period of convergence between the structural and fluid dynamics of the system.

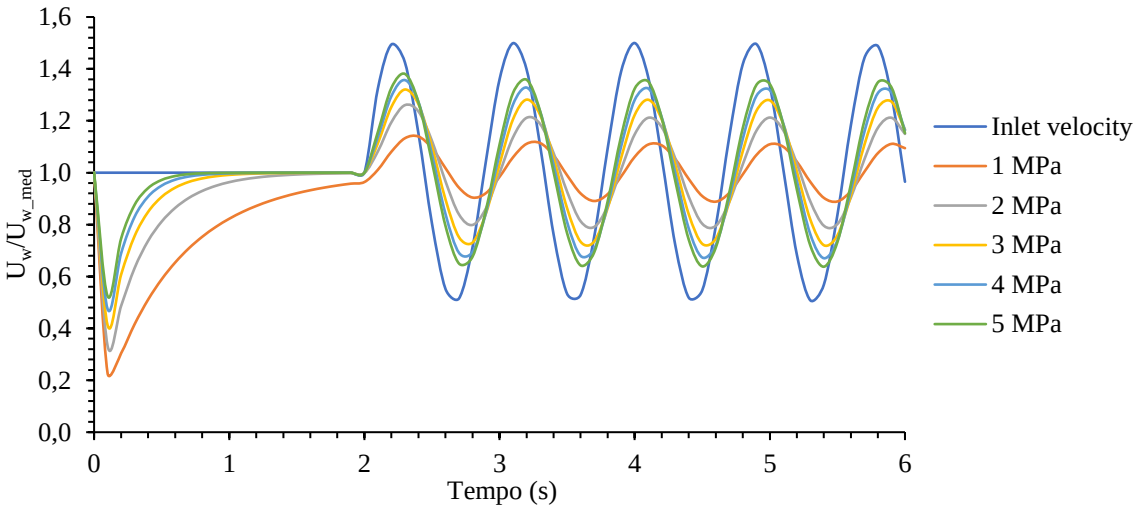

Figure 10. Comparison of normalized flows in relation to the mean at the inlet and outlet of the attenuator for different Young modulus.

The analysis of Figure 10 reveals that the reduction in the Young modulus of the material enables a decrease in the amplitude of the outflow, which is related to the greater capacity for volumetric variation. The simulation with Young modulus of 1 MPa presents the highest attenuation value, reaching approximately 76.65% of the inlet flow. Then, the simulations with Young modulus of 2 MPa, 3 MPa, 4 MPa and 5 MPa present attenuation values of 55.70%, 42.20%, 33.10% and 26.77%, respectively.

4. CONCLUSION

Through bidirectional numerical simulation of the transient fluid-structure interaction, it was possible to analyze the behavior of a resistive attenuator in a hydraulic line. The consistency between the numerical simulation results and those discussed in the literature indicates that the model was able to reliably reproduce the behavior of the resistive attenuator in question. Reducing the Young modulus of the material used in the attenuator resulted in a significant increase in the volumetric change rate, which in turn led to a greater reduction in inlet flow. The most expressive results indicated that the attenuator was able to attenuate the inlet flow by approximately 76.65%.

Furthermore, the influence of the Young modulus on the von Mises equivalent voltage of the resistive attenuator is observed. Reducing the Young modulus from 5 MPa to 1 MPa resulted in a 20.09% decrease in the maximum stress distribution. This reduction in voltage distribution can have important implications for the durability and performance of the resistive attenuator, as a lower voltage can indicate a reduced ability to withstand loads and stresses without failure.

The results highlight the importance of design and proper selection of materials in the development of efficient attenuators. By adjusting material properties, such as Young modulus, it is possible to influence the attenuator's ability to reduce fluid flow. The relationship between volumetric variation and attenuation level can depend on many factors, such as attenuator design, material properties, and operating conditions. Therefore, it is recommended that future work analyze the results in a broader context and consider other relevant variables for a complete understanding of the performance of flux attenuators.

5. REFERENCES

Beynart, L., 1999. Pulsation Dampening in Suction and Discharge Systems for PD Pumps. Elsevier Science Ltd, California, p. 20-24. Available in: <https://www.academia.edu/10034984/Pulsation_dampening_in_suction_and_discharge_systems_for_PD_pumps>.

Callister, W. D., 2007. Materials Science and Engineering: An Introduction. 7.ed. Nova Iorque: John Willey & Sons. 705 p.

Deng, R., Cheng, Y., Wang, C., 2012. Experiments and simulation on a pulse dampener system for stabilizing liquid flow**.** Chemical Engineering Journal**,** p. 136-142, nov. Elsevier BV. http://dx.doi.org/10.1016/j.cej.2012.08.083.

Flexodamp. Pulsation Dampers: Vibration Isolator. 2 p. (Manual de instrução). Available in: <https://www.flexodamp.com/en/pulmon-shockabsorber-pulsations/flexodamp-fd/#popmake-3014>.

Flowrox, 2015. Installation, Operation and Maintenance Instructions for Flowrox Expulse™ Dampener DN32 - DN100. Lappeenranta. 24 p. (Installation, operation and maintenance manual). Available in: < https://ablinternational.com.pe/wpcontent/uploads/2019/06/Expulse_Dumper_Manual.pdf>.

Hibbeler, R.C., 2000. Resistência dos Materiais, 3.ª Ed., Editora Livros Técnicos e Científicos.

Klas, R., Fialová, S., 2019. Pulse flow of liquid in flexible tube. Epj Web Of Conferences, v. 213, p. 02041. EDP Sciences. http://dx.doi.org/10.1051/epjconf/201921302041.

Koegler, A. F., Haselmann, D., Alt, N. S. A., Schluecker, E., 2016. Experimental Characterization of a Flow-through Pulsation Damper Regarding Pressure Pulsations and Vibrations. Chemical Engineering & Technology, v. 40, p. 162-169. Wiley. http://dx.doi.org/10.1002/ceat.201600175.

Macintyre, A. J., 1997. Equipamentos Industriais e de Processos. Rio de Janeiro: Livros Técnicos e Científicos Editora Ltda, 1997. 277 p.

Mei, C. C., Zhang, J., Jing, H. X., 2018. Fluid mechanics of Windkessel effect. Medical & Biological Engineering & Computing, v. 56, p. 1357-1366. Springer Science and Business Media LLC. http://dx.doi.org/10.1007/s11517-017-1775-y.

Oliveira, F. M., Huebner, R., Greco, M., 2016. Simulação de interação fluido-estrutura em dutos com escoamento interno utilizando software livre. Interdiciplinar de Pesquisa em Engenharia, Brasília, p. 1-18.

Shaaban, M., Mohany, A., 2015. Passive control of flow-excited acoustic resonance in rectangular cavities using upstream mounted blocks. Experiments in Fluids, v. 56, p. 56-72. Springer Science and Business Media LLC. http://dx.doi.org/10.1007/s00348-015-1908-8.

Shahzad, M., Kamran, A., Siddiqui, M. Z., Farhan, M., 2015. Mechanical Characterization and FE Modelling of a Hyperelastic Material. Materials Research, v. 18, p. 918-924. FapUNIFESP (SciELO). http://dx.doi.org/10.1590/1516-1439.320414.

Wachel, J. C., Price, S. M., 1988. Understanding How Pulsation Accumulators Work. American Society of Mechanical Engineers, Petroleum Division, n. 14, p. 23–31. Available in: <https://engdyn.com/resources/understanding-how-pulsation-accumulators-work/>.

Wang, Yan., Tongsheng, S., Chunsen, T., Jian, F., Shengrong, G., 2021. Research Status, Critical Technologies, and Development Trends of Hydraulic Pressure Pulsation Attenuator. Chinese Journal Of Mechanical Engineering, v. 34, p. 1-17. Springer Science and Business Media LLC. http://dx.doi.org/10.1186/s10033-021-00532-z.

6. RESPONSIBILITY NOTICE

The authors are the only responsible for the printed material included in this paper.